


## Influence of the electron density on the giant negative magnetoresistance in two-dimensional electron gases

L. Bockhorn<sup>1,\*</sup>, D. Schuh<sup>2</sup>, C. Reichl<sup>3</sup>, W. Wegscheider<sup>3</sup>, and R. J. Haug<sup>1</sup>

<sup>1</sup>*Institut für Festkörperphysik, Leibniz Universität Hannover, 30167 Hannover, Germany*

<sup>2</sup>*Institut für Experimentelle und Angewandte Physik, Universität Regensburg, 93053 Regensburg, Germany*

<sup>3</sup>*Laboratorium für Festkörperphysik, ETH Zürich, 8093 Zürich, Switzerland*

 (Received 22 September 2023; revised 8 February 2024; accepted 19 April 2024; published 13 May 2024)

*In situ* variation of the electron density via a metallic gate can control the disorder potentials in two-dimensional electron gases (2DEGs). This also influences the negative magnetoresistance at low magnetic fields, which is commonly observed in ultrahigh mobility 2DEGs. We investigate the temperature-dependent giant negative magnetoresistance (GNMR) as a function of the electron density for several temperatures and currents. Thereby, we find that the GNMR behavior depends decisively on the electron density. This observation is attributed to a changed disorder potential with electron density. In the case of higher electron densities, a nonlinear current dependency of the GNMR is observed, which could be described within the hydrodynamic regime.

DOI: [10.1103/PhysRevB.109.205416](https://doi.org/10.1103/PhysRevB.109.205416)

### I. INTRODUCTION

Two-dimensional electron gases (2DEGs) with ultrahigh mobility not only show an abundant number of fractional filling factors, but also an astonishingly robust negative magnetoresistance around  $B = 0$  T [1–9]. The theoretical description of this strong negative magnetoresistance is still an open issue as it involves several independent parameters, e.g., temperature, in-plane magnetic field, etc. Below 800 mK, some ultrahigh mobility 2DEGs show a very strong negative magnetoresistance which can be divided into two parts [3–6,8]: a temperature-independent narrow peak around  $B = 0$  T and a temperature-dependent giant negative magnetoresistance (GNMR) at larger magnetic fields up to  $B = 100$  mT. The narrow peak is robust against several external tuning parameters and originates from an interplay of smooth disorder and elastic scattering at macroscopic defects [6,8–13]. In contrast, the GNMR at larger magnetic fields is sensitive to a variety of different scatterings and interactions, which makes its theoretical description more complex.

Over the years, different theoretical models have been introduced to describe this GNMR. Initially the strong temperature dependence as well as its sensitivity to in-plane magnetic fields was described by an electron-electron interaction correction to the conductivity considering mixed disorder [3,4,6,14,15]. Regarding the dependence on the magnetic field and the applied current, a model based on elastic scattering

between Landau levels was also suggested [16]. Recently, the GNMR was described by interactions within a hydrodynamic model [17–20]. However, different groups reported on discrepancies between the published theoretical models and the observed GNMR [3–5,9].

In addition to experimental tuning parameters, the GNMR seems to be influenced by different scattering events, e.g., interface roughness, oval defects, background impurities, and remote ionized impurities, further complicating a complete theoretical description. The contribution of the different disorder potential changes with the electron density [21]. Therefore, we take a closer look at the electron density dependence of the GNMR in this article to narrow down the involved scattering mechanisms.

### II. EXPERIMENTAL SETUP

In the case of ultrahigh mobility samples, the layer structure is complex, and also distant Si doped layers influence the properties of the 2DEG. The investigated samples originate from two different ultrahigh mobility materials (A and B) with similar layer structures [6]. The layer structure of one GaAs/AlGaAs heterostructure is depicted in the left inset of Fig. 1. Here, the conduction band edge is illustrated from the surface down to 350 nm beneath the surface. Both 2DEGs are realized in a 30 nm wide GaAs quantum well (QW) at a depth of 170 nm and they are  $\delta$ -Si doped from both sides. The  $\delta$ -Si-doped GaAs layers are located at 80 nm and 260 nm beneath the surface and enclosed in AlAs layers. These doping layers form  $X$  minima in the conduction band which are also populated with free electrons. Additionally, two Si-donor layers are situated at about 40 nm and 600 nm. The electron density and the electron mobility is slightly different for both materials ( $n_{e,A} \approx 3.2 \times 10^{11} \text{ cm}^{-2}$  and  $n_{e,B} \approx 3.3 \times 10^{11} \text{ cm}^{-2}$ , respectively,  $\mu_A \approx 8.5 \times 10^6 \text{ cm}^2/\text{Vs}$  and  $\mu_B \approx 7.3 \times 10^6 \text{ cm}^2/\text{Vs}$ ).

\*bockhorn@nano.uni-hannover.de

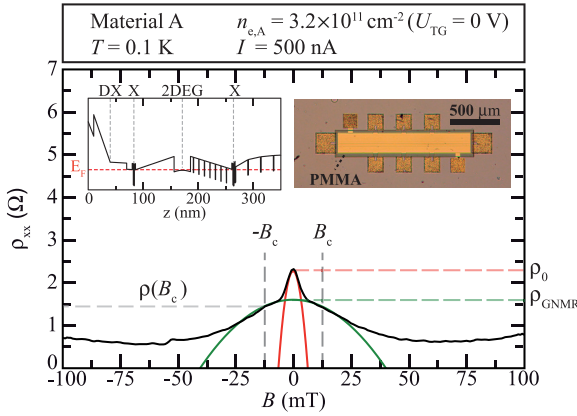


FIG. 1. The longitudinal resistivity  $\rho_{xx}$  against the magnetic field  $B$  in the range of the strong negative magnetoresistance. The strong negative magnetoresistance is divided into two sections fitted by parabolic magnetic field dependences, the GNMR (green parabola) and a narrow peak (red parabola). A plateau in the longitudinal resistivity around  $B_c = \pm 12.5$  mT marks the crossover between both regions. Inset (left): Calculated conduction band of our heterostructure down to 350 nm beneath the surface using the program *1D Poisson.exe* [22,23]. The 2DEGs is located in a 30 nm wide GaAs QW at a depth of 170 nm. Inset (right): Optical microscopy image of the Hall geometry. The metallic top gate is separated by a 600 nm thick PMMA layer.

Various samples were structured under comparable conditions. The samples were etched 360 nm deep to define a 1200  $\mu\text{m}$  long and 200  $\mu\text{m}$  wide Hall bar. The distance between two longitudinal ohmic contacts was 275  $\mu\text{m}$ . The Hall bars were defined by photolithography and wet chemical etching. In order to investigate the influence of the electron density on the negative magnetoresistance we fabricated a metallic top gate, which consists of 15 nm Au and 45 nm Ti. Since top-gate electrodes often result in unwanted strain and hysteresis effects, which decrease the sample quality, we added a layer of approximately 600 nm polymethylmethacrylate (PMMA) between the Hall bar and the metallic top gate to reduce the strain effect, and to separate the electrode from the surface, thus avoiding leakage currents. The resulting Hall geometry is shown in Fig. 1 (right inset). The low temperature magnetotransport measurements were performed in a dilution refrigerator with the electron temperature ranging from 100 mK to 800 mK. All measurements were carried out by using low-frequency (13 Hz) lock-in technique. The properties of both materials for gated samples are summarized in

TABLE I. Summary of the results of both ultrahigh mobility samples (A and B), which show a strong negative magnetoresistance. In addition to the electron density  $n_e$  and the mobility  $\mu_0$  based on  $\rho_0$ , we also determined the maximum of the GNMR curvature  $\rho_{\text{GNMR}}$  and its corresponding mobility  $\mu_{\text{GNMR}}$ . The quantum scattering time  $\tau_q$  is calculated from the magnitude of the Shubnikov-de Haas oscillations [24], while the transport scattering time for smooth disorder  $\tau_L$  is based on the plateau in the longitudinal resistivity. The density of the rare strong scatterers  $n_s$  are extracted from the peak curvature [6,8].

Material	$n_e$ [cm <sup>-2</sup> ]	$\rho_0$ [ $\Omega$ ]	$\rho_{\text{GNMR}}$ [ $\Omega$ ]	$\mu_0$ [cm <sup>2</sup> /Vs]	$\mu_{\text{GNMR}}$ [cm <sup>2</sup> /Vs]	$\tau$ [s]	$\tau_q$ [s]	$\tau_L$ [s]	$n_s$ [cm <sup>-2</sup> ]
A	$\approx 3.2 \times 10^{11}$	2.3	1.65	$8.5 \times 10^6$	$11.8 \times 10^6$	$3.2 \times 10^{-10}$	$1.8 \times 10^{-12}$	$5.0 \times 10^{-10}$	$1.3 \times 10^4$
B	$\approx 3.3 \times 10^{11}$	2.6	1.75	$7.3 \times 10^6$	$10.8 \times 10^6$	$2.8 \times 10^{-10}$	$1.2 \times 10^{-12}$	$4.2 \times 10^{-10}$	$1.1 \times 10^4$

Table I. In the following we take a closer look on the results of a gated sample of material A.

### III. THE NEGATIVE MAGNETORESISTANCE

The longitudinal resistivity  $\rho_{xx}$  shown in Fig. 1 focuses onto the magnetic field range of the strong negative magnetoresistance for a gated sample of material A at  $T = 0.1$  K and for an applied current of  $I = 500$  nA. For the condition  $U_{TG} = 0$  V, an electron density of  $n_{e,A} = 3.2 \times 10^{11}$  cm<sup>-2</sup> was detected. In Fig. 1, the strong negative magnetoresistance consists of two contributions with parabolic magnetic field dependencies: a GNMR spanning larger magnetic fields (green parabola) and a narrow peak around zero magnetic field (red parabola) [3–6,8]. A slight plateau in the longitudinal resistivity around  $B_c = \pm 12.5$  mT marks the crossover between the peak and the GNMR [6,8]. Also marked in Fig. 1 is the maximum of the peak  $\rho_0$  and the maximum of the GNMR curvature  $\rho_{\text{GNMR}}$ .

The narrow peak is robust against several parameters and originates from an interplay of smooth disorder and elastic scattering on macroscopic defects [6,8–11], e.g., GaAs droplets. Two parameters, the height of the peak and its curvature, fully describe the peak. The height of the peak  $\Delta\rho_{xx} = \rho_0 - \rho_{xx}(B_c)$  is given by the difference between the longitudinal resistivity at zero magnetic field  $\rho_0$  and the value of the plateau  $\rho_{xx}(B_c)$ . The curvature of the peak  $C_{\text{peak}}$  is determined by fitting a parabola to the experimental data. These values can be compared with the theoretical model of the peak expressed by [6,8,10]

$$\rho_{xx} = \rho_0 - \rho_0 \frac{\omega_c^2}{2\pi n_s v_F^2} f(x), \quad (1)$$

where  $\omega_c = eB/m^*$  is the cyclotron frequency,  $v_F$  is the Fermi velocity, and  $f(x)$  is given by

$$f(x) = \frac{2}{x+1} \int_0^\infty dq \frac{q J_1^2(q)}{xq^2 + 2[1 - J_0^2(q)]} \quad (2)$$

with  $x = \rho_{xx}(B_c) \times \Delta\rho_{xx}^{-1}$ , and  $J_{0,1}(q)$  as Bessel functions. The only free parameter in Eq. (1) is the density of the rare strong scatterers  $n_s$  which were identified as macroscopic growth defects [6,8]. From the data in Fig. 1, we determined a density of strong scatterers of  $n_s = 1.3 \times 10^4$  cm<sup>-2</sup> based on a peak curvature of  $C_{\text{peak}} = 55$  k $\Omega$  m<sup>4</sup>/(V s)<sup>2</sup>.

Recently, it was demonstrated that the plateau in the longitudinal resistivity around  $B_c = \pm 12.5$  mT is dominated by smooth disorder [6,8]. This value thus allows us to

extract the transport scattering time for smooth disorder via  $\tau_L = m^*/(e^2 n_e \rho_{xx}(B_c))$ , and we obtain  $\tau_L = 5.0 \times 10^{-10}$  s. The transport scattering time for smooth disorder could be also extracted from the quantum scattering time  $\tau_q$  and the spacer width via  $\tau_{sm} = (k_F d)^2 \tau_q$ . Due to the fact that the quantum scattering time is calculated from the magnitude of the Shubnikov-de Haas oscillations following Coleridge *et al.* [24], the corresponding transport scattering time  $\tau_{sm}$  could be influenced by inhomogeneities in the electron density and an additional occupied sub-band in the QW [3,6]. Therefore, we rely in the following on the transport scattering for smooth disorder  $\tau_L$  extracted from the plateau in the longitudinal resistivity.

To compare our observations of the GNMR with theoretical models we refer to the electron-electron interaction correction to the conductivity  $\delta\sigma_{xx}^{ee}(T)$  [3,14,25,26]. In accordance with Ref. [15] we assume a model of mixed disorder for the characterization of the GNMR. In the case of ballistic transport and for strong magnetic fields, smooth disorder (e.g., ionized donors in the doping layers) is the dominating disorder contribution, which is in accordance with our observations for the narrow peak around zero magnetic field. The GNMR is then expressed by

$$\rho_{xx} = \rho_{\text{GNMR}} - \frac{2 c_0}{n_e^2 \pi^2 \sqrt{\hbar} \tau k_B T} \times \sqrt{\frac{\tau_L}{\tau}} \times B^2 \quad (3)$$

with  $c_0 = 0.276$  and  $\rho_{\text{GNMR}}$ . The second term of Eq. (3) describes the curvature  $C_{\text{GNMR}}$  of the GNMR. In our example we calculated a GNMR curvature of  $C_{\text{GNMR}} = 38 \Omega \text{ m}^4 / (\text{V s})^2$  taking a transport scattering time of  $\tau = 3.2 \times 10^{-10}$  s into account. However, the GNMR curvature obtained from the experimental data is much larger,  $C_{\text{GNMR}} = 970 \Omega \text{ m}^4 / (\text{V s})^2$ , as reported also before [3]. This discrepancy can be rationalized by additional contributions to the resistivity correction, such as unconsidered disorder potentials or scattering events in the hydrodynamic regime [17–20].

Hydrodynamic phenomena are expected when the electron-electron scattering length  $\ell_{ee}$  is much smaller than the sample width  $w$ . The electron-electron scattering length can be estimated through a model developed by Giuliani and Quinn [27]. In our example, we calculate from this model an electron-electron scattering length of  $\ell_{ee}^{GQ} = 0.014$  m, which is much larger than our sample width. Thus, scattering events in the hydrodynamic regime should be negligible for the description of our GNMR if we consider Giuliani and Quinn [27]. On the other hand, we see that electron-electron interaction plays a crucial role in describing the GNMR. For this reason, we do not want to exclude scattering in the hydrodynamic regime and consider an approach to hydrodynamic transport suitable for our 2DEG. Recently, Gornyi and Polyakov [12] describe the electron flow in the hydrodynamic regime in the presence of randomly distributed rare impenetrable scatterers and magnetic field, which would be consistent with our observations. This description includes a viscosity-modulated negative magnetoresistance of a Lorentzian shape expressed by

$$\frac{\rho_{xx}(B) - \rho_{\text{GNMR}}}{\rho_{\text{GNMR}}} \simeq - \frac{(2 \omega_c \tau_{ee}^{\text{GNMR}})^2}{1 + (2 \omega_c \tau_{ee}^{\text{GNMR}})^2}. \quad (4)$$

This equation yields an electron-electron scattering time  $\tau_{ee}^{\text{GNMR}}$  and we can extract a scattering length of  $\ell_{ee}^{\text{GNMR}} = 1.4 \times 10^{-6}$  m from the GNMR curvature, which would be the smallest length scale in our problem.

#### IV. THE GIANT NEGATIVE MAGNETORESISTANCE AS A FUNCTION OF ELECTRON DENSITY

In the following, we analyze the GNMR for different electron densities to get a deeper insight into the discrepancy between theory and experimental data. In addition, we want to understand if scattering in the hydrodynamic regime is a relevant parameter to describe the GNMR. Figure 2(a) shows the longitudinal resistivity  $\rho_{xx}$  as a function of the magnetic field  $B$  in the range of the strong negative magnetoresistance for several electron densities. Here, the electron density was lowered from  $n_{e,A} = 3.2 \times 10^{11} \text{ cm}^{-2}$  to  $1.9 \times 10^{11} \text{ cm}^{-2}$  in 12 steps, while the temperature  $T = 0.1$  K and the applied current  $I = 500$  nA were kept constant. As seen in Fig. 2(a), the strong negative magnetoresistance becomes more pronounced as the electron density decreases.

First, we investigate the influence of a negative gate voltage on our ultrahigh mobility 2DEG. A negative voltage on the metallic top gate causes a bending of the conduction band and the wave function of the 2DEG is shifted to the lower part of the GaAs QW. Hence, by decreasing the electron density the influence of the disorder potential landscape below the GaAs QW becomes stronger. Huang *et al.* [21] recently showed that the scattering mechanism depends on the electron density in ultrahigh mobility samples. In the situation of higher electron densities ( $n_e > 1 \times 10^{11} \text{ cm}^{-2}$ ), scattering on interface roughness is the dominant disorder potential, while for lower electron densities the influence of background impurities increase. Additionally, not only is the 2DEG depleted by decreasing the gate voltage but also the upper  $X$  minimum, which could also influence the magnetotransport measurements. In Fig. 2(b), the electron density  $n_{e,A}$  (blue circles) and the mobility  $\mu_A$  (red squares) are illustrated as a function of gate voltages at  $T = 0.1$  K. In the range from  $U_{TG} = -6$  V to 0 V, the electron density increases linearly with the gate voltage, only below  $U_{TG} = -6$  V one observes a saturation due to charge redistribution in the region between the metallic gate and the 2DEG during depletion [28]. Based on the observed gate-induced ionization of the upper  $X$  minimum, one can assume a gate-dependent disorder potential which strongly affects the development of the GNMR.

To analyze the narrow peak and the GNMR in more detail, we determine its curvatures  $C_{\text{peak}}$  and  $C_{\text{GNMR}}$  as a function of the electron density. Therefore, we fit a parabola of the form  $\rho_{xx} = \rho_0 - C_{\text{peak}} \times B^2$  to the experimental data of the narrow peak, while the experimental data of the GNMR is expressed by  $\rho_{xx} = \rho_{\text{GNMR}} - C_{\text{GNMR}} \times B^2$ . In Fig. 2(c), the results for both curvatures are plotted as a function of the electron density. Here, it becomes clear that the curvature of the GNMR (colored dots) is independent of the electron density  $n_e$  for the considered range, while the peak curvature (black triangles) varies. Regarding the expression of the narrow peak an increase of the peak width by reducing the electron density  $n_e$  is expected for a fixed density of strong scatterers  $n_s$  [see Eq. (1)]. While the theory of the narrow peak

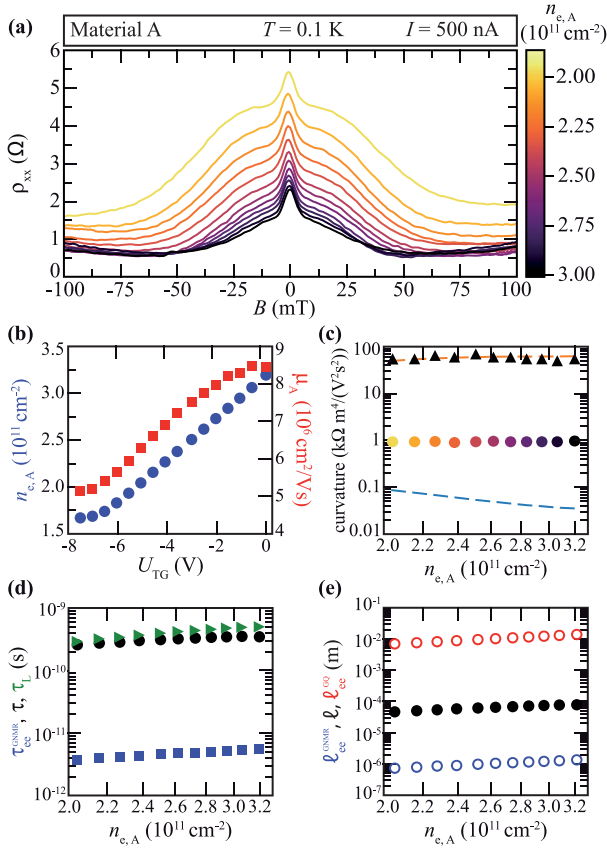


FIG. 2. (a) The longitudinal resistivity  $\rho_{xx}$  against the magnetic field  $B$  in the range of the strong negative magnetoresistance for different electron densities  $n_e$ . The GNMR gets more pronounced as the electron density decreases, while the narrow peak around  $B = 0$  T is left unchanged. (b) The electron density  $n_e$  (circles) and the mobility  $\mu_e$  (squares) as a function of the gate voltages  $U_{TG}$ . For gate voltages smaller than  $U_{TG} = -6$  V a plateau is observed due to charge redistribution. (c) The GNMR curvatures (colored circles), the peak curvatures (black triangles), as well as their theoretically predicted values are shown as functions of the electron density  $n_e$ . The GNMR curvature seems to be independent of the electron density  $n_e$ , which is in contrast to the predicted theoretical behavior (blue dashed line) [15]. The determined peak curvatures are in the range of the theoretical predicted values (orange dashed line). (d) Different transport scattering times extracted from the experimental data as a function of the electron density  $n_e$ . We determined the transport scattering time  $\tau$  (black circle), the electron-electron scattering time  $\tau_{ee}^{GNMR}$  (blue squares), and the transport scattering time for smooth disorder  $\tau_L$  (green triangle) [6,10]. (e) The mobility mean-free path  $\ell$  (black circles), the electron-electron scattering lengths  $\ell_{ee}^{GQ}$  (red circles) [27], and  $\ell_{ee}^{GNMR}$  (blue circles) [12] against the electron density  $n_e$ .

(orange dashed line) captures nicely the experimental data, the predicted GNMR curvature calculated from Eq. (3) (blue dashed line) is much smaller than the one extracted from the experimental data, see Fig. 2(c). Instead of an electron density dependence, a constant value is observed. Consequently, the used theoretical model [see Eq. (3)] does not capture the essence of the GNMR. The reasons for this discrepancy could be that the disorder potential depends on the electron density which is not considered much by theory.

From the longitudinal resistivity for different electron densities we extracted the transport scattering time  $\tau$  based on  $\rho_0$  and the transport scattering time for smooth disorder  $\tau_L$  calculated from the plateau in the longitudinal resistivity around  $B_c = \pm 12.5$  mT. We also determined the electron-electron scattering time  $\tau_{ee}^{GNMR}$  for each electron density through Eq. (4). In Fig. 2(d), the different transport scattering times are plotted against the electron density, the transport scattering time  $\tau$  (black circle), the electron-electron scattering time  $\tau_{ee}^{GNMR}$  (blue squares), and the transport scattering time for smooth disorder  $\tau_L$  (green triangle). The transport scattering time  $\tau$  is proportional to  $n_e^{3/2}$ . Also a clear dependency of the electron-electron scattering time  $\tau_{ee}^{GNMR}$  on the electron density is observed. Interestingly, the electron-electron scattering time  $\tau_{ee}^{GNMR}$  is proportional to  $n_e$ .

Finally, we also determine the mobility mean-free path  $\ell$  and the electron-electron scattering lengths  $\ell_{ee}^{GQ}$  [27] and  $\ell_{ee}^{GNMR}$  [12] as a function of the electron density, see Fig. 2(e). Whereas the mean-free path  $\ell$  is on the order of the sample size, the electron-electron scattering length  $\ell_{ee}^{GQ}$  considering [27] is much larger for all electron densities. In contrast,  $\ell_{ee}^{GNMR}$  extracted from Eq. (4) is smaller than the sample width. Regarding  $\ell_{ee}^{GNMR}$ , scattering in the hydrodynamic regime should be considered by describing the GNMR. For samples with smooth sidewalls Keser *et al.* [29] observed a strong electron density dependence of the electron-electron scattering length  $\ell_{ee}$  at 20 K. The electron-electron scattering length is reduced by decreasing the electron density, which agrees with our observation. In order to get an idea of a possible influence of different scattering regimes, we analyze the GNMR in the following for two different electron densities for different parameters. Therefore, we chose the situation for no applied top-gate voltage  $U_{TG} = 0$  V to show the unaffected disorder potential landscape of the sample, and for a lower top-gate voltage  $U_{TG} = -4$  V before a saturation due to charge redistribution is observed to represent the situation for a bent conduction band.

### A. Temperature dependence of the giant negative magnetoresistance

First, we take a look on the strong temperature dependence of the GNMR. Figure 3 shows the temperature dependence of the GNMR for two different electron densities, (a)  $n_{e,A} = 2.3 \times 10^{11} \text{ cm}^{-2}$  and (b)  $n_{e,A} = 3.2 \times 10^{11} \text{ cm}^{-2}$ . Here, the longitudinal resistivity  $\rho_{xx}$  is plotted against the magnetic field  $B$  for several temperatures  $T$ , which were increased from 0.1 K to 0.8 K in 11 steps while the applied current was kept constant  $I = 500$  nA. The GNMR vanishes with higher temperature  $T$  for both electron densities, while the narrow peak around zero magnetic field is left unchanged. To analyze the influence of the temperature on the GNMR in more detail we determine its curvature. At the lower electron density,  $n_{e,A} = 2.3 \times 10^{11} \text{ cm}^{-2}$ , two different temperature regimes can be clearly distinguished, see Fig. 3(a) (right). Above 0.3 K a  $T^{-1}$  dependency is observed for the GNMR curvature while for lower temperatures a  $T^{-1/2}$  dependency is determined. The latter is in line with the electron-electron interaction correction considering mixed disorder [14,15], see Eq. (3).

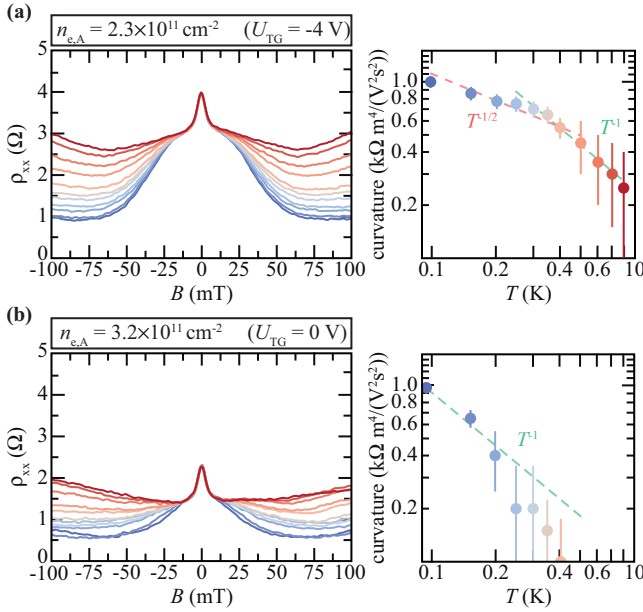


FIG. 3. (left) The strong negative magnetoresistance as a function of magnetic field  $B$  and temperature  $T$  for two different electron densities (a)  $n_{e,A} = 2.3 \times 10^{11} \text{ cm}^{-2}$  and (b)  $n_{e,A} = 3.2 \times 10^{11} \text{ cm}^{-2}$ . For both electron densities, the GNMR shows a strong temperature dependence, while the narrow peak around zero magnetic field is left unchanged. (right) The determined GNMR curvatures as a function of the temperature for (a)  $n_{e,A} = 2.3 \times 10^{11} \text{ cm}^{-2}$  and (b)  $n_{e,A} = 3.2 \times 10^{11} \text{ cm}^{-2}$ . For the lower electron density,  $n_{e,A} = 2.3 \times 10^{11} \text{ cm}^{-2}$ , two different temperature regimes are clearly visible. In the case of the higher electron density,  $n_{e,A} = 3.2 \times 10^{11} \text{ cm}^{-2}$ , a temperature dependence of roughly  $T^{-1}$  can be estimated.

In the situation of the higher electron density  $n_{e,A} = 3.2 \times 10^{11} \text{ cm}^{-2}$ , see Fig. 3(b), the curvature is hard to determine for temperatures above  $T = 0.2 \text{ K}$ . A temperature dependence of roughly  $T^{-1}$  can be estimated for the lower temperatures, which we observe for the lower electron density  $n_{e,A} = 2.3 \times 10^{11} \text{ cm}^{-2}$  above  $0.3 \text{ K}$ . The different temperature dependencies may have their origin in the fact that the influence of the interface roughness is stronger for higher electron densities [21], while the influence of background impurities increases by decreasing the electron density, which leads to a different disorder potential. Already, Ref. [15] showed that a changed disorder potential leads to a different temperature dependency. Despite the predicted temperature dependencies for lower electron densities, we still observe a discrepancy between the experimental data and the interaction-induced resistivity correction [3]. From this, we conclude that by increasing the electron density the disorder potential landscape is more complex as assumed.

### B. Current dependence of the giant negative magnetoresistance

An alternative route to reducing the electron-electron scattering length  $\ell_{ee}$  and changing transport characteristics from ballistic to hydrodynamic is through increasing the applied current  $I$  [30]. In another measurement cycle including a new cool down of the sample, we also examined the

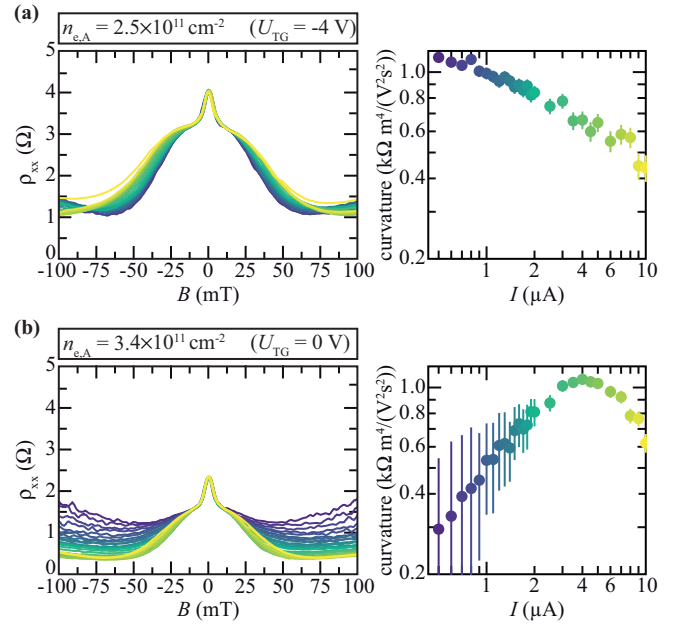


FIG. 4. (left) The strong negative magnetoresistance as a function of magnetic field  $B$  and current  $I$  for two different electron densities (a)  $n_{e,A} = 2.5 \times 10^{11} \text{ cm}^{-2}$  and (b)  $n_{e,A} = 3.4 \times 10^{11} \text{ cm}^{-2}$ . The current dependence of the GNMR is different for both electron densities, while the narrow peak is left unchanged. (right) The determined GNMR curvatures as a function of the current  $I$  for (a)  $n_{e,A} = 2.5 \times 10^{11} \text{ cm}^{-2}$  and (b)  $n_{e,A} = 3.4 \times 10^{11} \text{ cm}^{-2}$ . In the case of the lower electron density,  $n_{e,A} = 2.5 \times 10^{11} \text{ cm}^{-2}$ , a heating effect due to the increased current can be assumed. For the higher electron density,  $n_{e,A} = 3.4 \times 10^{11} \text{ cm}^{-2}$ , a clear nonlinear current dependence is observed.

current dependent behavior of the GNMR. Therefore, we gradually increased the amplitude of the lock-in amplifier between the individual measurements. After each measurement cycle, the sample has to warm up to room temperature because the higher AC currents irreversibly changed the 2DEG. Since the necessary warm ups lead to a change in the sample quality, the selected electron densities differ slightly from the previous ones. In the following, we examine the current dependence of the GNMR for two different electron densities. Again, we chose the situation for no applied top-gate voltage,  $U_{TG} = 0 \text{ V}$ , to show the unaffected disorder potential landscape of the sample, and for a lower top-gate voltage,  $U_{TG} = -4 \text{ V}$ . In Fig. 4 (left) the longitudinal resistivity  $\rho_{xx}$  is shown as a function of the magnetic field  $B$  in the range of the strong negative magnetoresistance for several currents  $I$  for (a)  $n_{e,A} = 2.5 \times 10^{11} \text{ cm}^{-2}$  and (b)  $n_{e,A} = 3.4 \times 10^{11} \text{ cm}^{-2}$ . The current  $I$  is increased from  $0.5 \mu\text{A}$  to  $10 \mu\text{A}$  in several steps. Immediately noticeable is that the current dependence of the GNMR is very different for the two considered electron densities, while the narrow peak is left unchanged in both cases. To analyze the behavior of the GNMR in more detail, we determine its curvature for both electron densities, shown in Fig. 4 (right).

In the situation of the lower electron density  $n_{e,A} = 2.5 \times 10^{11} \text{ cm}^{-2}$ , Fig. 4(a), the GNMR starts to broaden by increasing the current  $I$ . This is also reflected by its curvature.

Here, the value of the curvature  $C_{\text{GNMR}}$  decreases with the current  $I$ , showing a decrease in the electron-electron scattering time  $\tau_{ee}^{\text{GNMR}}$ . These observations could hint toward a growing importance of hydrodynamic contribution. Although, a heating effect due to the higher current cannot be excluded.

For a higher electron density  $n_{e,A} = 3.4 \times 10^{11} \text{ cm}^{-2}$ , see Fig. 4(b), the GNMR behaves completely different. Here, the GNMR gets more pronounced by increasing the current till  $I = 4 \mu\text{A}$ . Above  $I = 4 \mu\text{A}$  the GNMR broadens with increasing current. This nonlinear behavior is also reflected by its curvature. A maximum of the curvature is clearly observed around  $I = 4 \mu\text{A}$ . Recently, this nonlinear behavior of the GNMR was described by elastic scattering between Landau levels [31]. This nonlinear current dependency of the GNMR could be also caused by scattering in the hydrodynamic regime. Interestingly, the electron-electron scattering time  $\tau_{ee}^{\text{GNMR}}$  increases with current and reaches a maximum for  $I = 4 \mu\text{A}$  before it drops for larger currents. However, the occupation of a second sub-band for higher electron densities could be also responsible for the nonlinear current dependency.

## V. DISCUSSION AND SUMMARY

Regarding the electron density dependent measurements of the GNMR for different parameters, the theoretical description of the GNMR is complex and must involve different scattering regimes and a material specific disorder potential. The observed temperature dependence of  $T^{-1/2}$  of the GNMR for the lower electron density  $n_{e,A} = 2.5 \times 10^{11} \text{ cm}^{-2}$  is predicted by the electron-electron interaction correction to the conductivity [15]. However, there is still a discrepancy between the experimental data and this theoretical model maybe caused by additional scattering events like interface

roughness or background impurities. The nonlinear current dependency of the GNMR for the higher electron density  $n_{e,A} = 3.4 \times 10^{11} \text{ cm}^{-2}$  points in the direction of scattering in the hydrodynamic regime as a further contribution but could be also a sign for the occupation of a second sub-band.

To conclude, we analyzed the GNMR of an ultrahigh mobility 2DEG for different electron densities  $n_e$  via a metallic gate. Remarkably, it seems that the curvature of the GNMR is independent of the electron density, which is in contrast to the predicted theoretical models. Therefore, we investigate the GNMR as a function of the electron density  $n_e$  for several temperatures  $T$  and currents  $I$ . For the chosen parameters, the appearance of the GNMR depends on the electron density. This suggests that the scattering potentials changed with the electron density as reported before by Huang *et al.* [21], which is not considered in theoretical models. From the GNMR under different conditions we also extracted the electron-electron scattering time  $\tau_{ee}^{\text{GNMR}}$  using the hydrodynamic expression as in Ref. [12], see Eq. (4), which interestingly appears to be proportional to the electron density  $n_e$ . In addition, the observed nonlinear current dependency of the GNMR could be described within the hydrodynamic regime [17–20]. Therefore, a hydrodynamic contribution to the GNMR should be also taken into account.

The data that support the findings of this study are available from the corresponding author upon reasonable request.

## ACKNOWLEDGMENTS

We would like to thank I. V. Gornyi and D. Wulferding for discussions and comments. This project has been funded by the Deutsche Forschungsgemeinschaft (DFG, German Research Foundation) under Germany's Excellence Strategy – EXC-2123 QuantumFrontiers – 390837967.

- 
- [1] Y. Dai, R. R. Du, L. N. Pfeiffer, and K. W. West, *Phys. Rev. Lett.* **105**, 246802 (2010).
  - [2] A. T. Hatke, M. A. Zudov, L. N. Pfeiffer, and K. W. West, *Phys. Rev. B* **84**, 121301(R) (2011).
  - [3] L. Bockhorn, P. Barthold, D. Schuh, W. Wegscheider, and R. J. Haug, *Phys. Rev. B* **83**, 113301 (2011).
  - [4] A. T. Hatke, M. A. Zudov, J. L. Reno, L. N. Pfeiffer, and K. W. West, *Phys. Rev. B* **85**, 081304(R) (2012).
  - [5] R. G. Mani, A. Kriisa, and W. Wegscheider, *Sci. Rep.* **3**, 2747 (2013).
  - [6] L. Bockhorn, I. V. Gornyi, D. Schuh, C. Reichl, W. Wegscheider, and R. J. Haug, *Phys. Rev. B* **90**, 165434 (2014).
  - [7] Q. Shi, M. A. Zudov, L. N. Pfeiffer, and K. W. West, *Phys. Rev. B* **90**, 201301(R) (2014).
  - [8] L. Bockhorn, A. Velieva, S. Hakim, T. Wagner, E. P. Rugeramigabo, D. Schuh, C. Reichl, W. Wegscheider, and R. J. Haug, *Appl. Phys. Lett.* **108**, 092103 (2016).
  - [9] B. Horn-Cosfeld, J. Schluck, J. Lammert, M. Cerchez, T. Heinzl, K. Pierz, H. W. Schumacher, and D. Mailly, *Phys. Rev. B* **104**, 045306 (2021).
  - [10] A. D. Mirlin, D. G. Polyakov, F. Evers, and P. Wölfle, *Phys. Rev. Lett.* **87**, 126805 (2001).
  - [11] D. G. Polyakov, F. Evers, A. D. Mirlin, and P. Wölfle, *Phys. Rev. B* **64**, 205306 (2001).
  - [12] I. V. Gornyi and D. G. Polyakov, *Phys. Rev. B* **108**, 165429 (2023).
  - [13] P. S. Alekseev and A. P. Dmitriev, *Phys. Rev. B* **108**, 205413 (2023).
  - [14] I. V. Gornyi and A. D. Mirlin, *Phys. Rev. Lett.* **90**, 076801 (2003).
  - [15] I. V. Gornyi and A. D. Mirlin, *Phys. Rev. B* **69**, 045313 (2004).
  - [16] J. Iñarrea, *Europhys. Lett.* **106**, 47005 (2014).
  - [17] P. S. Alekseev, *Phys. Rev. Lett.* **117**, 166601 (2016).
  - [18] P. S. Alekseev and M. A. Semina, *Phys. Rev. B* **98**, 165412 (2018).
  - [19] P. S. Alekseev and A. P. Dmitriev, *Phys. Rev. B* **102**, 241409(R) (2020).
  - [20] A. N. Afanasiev, P. S. Alekseev, A. A. Greshnov, and M. A. Semina, *Phys. Rev. B* **104**, 195415 (2021).

- [21] Y. Huang, B. I. Shklovskii, and M. A. Zudov, *Phys. Rev. Mat.* **6**, L061001 (2022).
- [22] G. L. Snider, I.-H. Tan, and E. L. Hu, *Appl. Phys.* **68**, 2849 (1990).
- [23] I.-H. Tan, G. L. Snider, and E. L. Hu, *Appl. Phys.* **68**, 4071 (1990).
- [24] P. T. Coleridge, R. Stoner, and R. Fletcher, *Phys. Rev. B* **39**, 1120 (1989).
- [25] M. A. Paalanen, D. C. Tsui, and J. C. M. Hwang, *Phys. Rev. Lett.* **51**, 2226 (1983).
- [26] L. Li, Y. Y. Proskuryakov, A. K. Savchenko, E. H. Linfield, and D. A. Ritchie, *Phys. Rev. Lett.* **90**, 076802 (2003).
- [27] G. F. Giuliani and J. J. Quinn, *Phys. Rev. B* **26**, 4421 (1982).
- [28] C. Rössler, T. Feil, P. Mensch, T. Ihn, K. Ensslin, D. Schuh, and W. Wegscheider, *New J. Phys.* **12**, 043007 (2010).
- [29] A. C. Keser, D. Q. Wang, O. Klochan, D. Y. H. Ho, O. A. Tkachenko, V. A. Tkachenko, D. Culcer, S. Adam, I. Farrer, D. A. Ritchie, O. P. Sushkov, and A. R. Hamilton, *Phys. Rev. X* **11**, 031030 (2021).
- [30] Z. T. Wang, M. Hilke, N. Fong, D. G. Austing, S. A. Studenikin, K. W. West, and L. N. Pfeiffer, *Phys. Rev. B* **107**, 195406 (2023).
- [31] J. Iñarrea, L. Bockhorn and R. J. Haug, *Europhys. Lett.* **115**, 17005 (2016).